LBNL-45198
ATL-PHYS-2000-016

Model Independent Extra-dimension signatures with ATLAS*

L. Vacavant and I. Hinchliffe
Lawrence Berkeley National Laboratory, Berkeley, CA

Abstract

The generic missing transverse energy signals at LHC for theories having large extra dimensions are discussed. Final states of jets plus missing energy and photons plus missing energy are simulated in the ATLAS detector. The discovery limit of LHC and the methods to determine the parameters of the underlying model are discussed.

*This work was supported in part by the Director, Office of Science, Office of High Energy and Nuclear physics, Division of High Energy Physics of the U.S. Department of Energy under Contract DE-AC03-76SF00098.

Contents

1 Introduction

There is much recent theoretical interest in models of particle physics that have extra-dimensions in addition to the 3+1 dimensions of normal space-time [1], [2]. In these models, new physics can appear at a mass scale of order 1 TeV and can therefore be accessible at LHC. The standard model has a large hierarchy of scales that exists between the mass scale of the weak interactions, set by the Fermi constant G_F (or the W-mass, M_W), and that of gravity, set by Newton's constant G_N (or the Planck Mass. $M_P \sim 10^{19}$ GeV). It is believed that a consistent quantum theory of gravity must be a string theory [3] which requires additional dimensions in order to be self-consistent. String theory has some inherent scale, the string scale M_S, associated with it. The additional dimensions must be compactified on some scale R so that they are currently unobserved. It is often assumed that $M_s \sim M_P \sim 1/R$ so that new physics would not be visible until these huge energy scales are reached. This type of model offers no insight as to the origin of the large hierarchy although it can, since the theory is supersymmetric, ensure that the hierarchy is stable with respect to quantum corrections.

Recently however it has been suggested that R could be much larger, allowing the fundamental scale of gravity, here called M_D, to be close to M_W and so remove the large hierarchy of scales [1]. If there are δ additional dimensions of size R, then the observed Newton constant is related to the fundamental scale M_D by

$$G_N = 8\pi R^\delta M_D^{-(2+\delta)}$$

If $M_D \sim 1$ TeV then $R \sim 10^{32/\delta - 16}$ mm implying that, if $\delta \geq 2$, R is smaller than the scales of order 1 mm down to which gravitational interactions have been probed. In this picture the apparent weakness of observed gravity is due to its dilution by the spreading of its field into the additional dimensions.[†]

When an extra dimension is compactified with size R, say on a circle, particles propagating exclusively in the extra dimensions appear, from a four dimensional viewpoint, as a tower of massive states. The characteristic mass splitting of these (Kaluza-Klein) states is of order $1/R$. In particular, gravitons propagating in the extra dimensions will appear to be massive states whose coupling to ordinary matter is determined only by gravitational interactions and is therefore known. However, the Standard model particles cannot be allowed to propagate into the extra dimensions as there is no "excited electron" with mass below a 100 GeV. New physics is expected to appear at a scale M_D; the details of this physics are model dependent.

This paper is concerned primarily with the model independent signatures and their observability in the ATLAS detector. Some remarks about the more model dependent signatures appear in the conclusion.

2 Graviton direct production

The emission of gravitons in particle collisions is calculable in terms of the universal coupling of gravity to all matter (G_N). The calculations become unreliable once energies comparable to the fundamental scale of gravity are reached. (Similarly, calculations in the Fermi theory of weak interactions become unreliable at energy scales of order M_W.) In the Standard Model, this energy is M_P, in the models with extra dimensions, it is M_D. In addition to the emission of massless gravitons, the Kaluza-Klein excitations that have mass differences of order $1/R$ can also be emitted

[†]It should be noted that the hierarchy problem is not solved in the simplest implementation of the idea; the large ratio M_P/M_W is replaced by the large value of RM_D whose origin is not explained.

and their rate calculated as their coupling to ordinary matter is also determined. For experiments involving the collision of particles whose energy is much larger than this mass splitting, the discrete spectrum can be approximated by a continuum with a density of states $dN/dm \sim m^{\delta-1}$. Since these emitted gravitons interact very weakly with ordinary matter, their emission gives rise to missing transverse energy signatures.

2.1 Sub-processes and cross-section

The relevant processes for LHC are $gg \to gG$, $qg \to qG$ and $q\overline{q} \to Gg$ which give rise to final states of jets plus missing E_T and $q\overline{q} \to G\gamma$ which gives rise to final states with a photon plus missing E_T. Final states of Z plus missing E_T are not considered as the effective rates are much lower since the Z can only be observed at LHC via its leptonic decay.

The relevant partonic cross sections can be written in the form $\frac{d^2\sigma}{dtdm}$ where m is the mass of the recoiling (Kaluza-Klein) graviton and $t = (p_a - p_f)^2$ is the usual Mandelstam variable (a represents and incoming parton and f the outgoing quark, gluon or photon).

The differential cross-section can be expressed in the following form:

$$\frac{d^4\sigma}{dm^2 dp^2_{T_{jet,\gamma}} dy_{jet,\gamma} dy_G} = \frac{m_G^{\delta-2}}{2} \frac{S_{\delta-1}}{M_D^{\delta+2}} \frac{d\sigma_m}{dt} \sum_{i,j} \frac{f_i(x_1)}{x_1} \frac{f_j(x_2)}{x_2} \tag{1}$$

where the partonic cross-sections $\frac{d\sigma_m}{dt}$ are given by [4] (eqs. 64-67)[‡]. $S_{\delta-1}$ is the surface of a unit-radius sphere in δ dimensions and $f_i(x)$ are the parton structure functions. It is important to notice that the fundamental scale M_D is factorized in Eqn. 1: $\sigma \propto M_D^{-\delta-2}$. A change of δ in this term can be compensated by a change of M_D. Unfortunately, disentangling M_D and δ is difficult. There is some dependence of δ induced by the kinematic limit on the partonic subprocess which implies a limit on the largest value of the emitted graviton mass m_G that can enter; this is discussed in section 5 where the variation of the rates with the LHC energy is discussed. This cross-section is only valid at energies low compared to M_D. At higher energies, new physics enters and modifies the result. This new physics is model dependent.

2.2 Implementation in ISAJET

For the purposes of this simulation, the relevant subprocesses have been implemented in ISAJET [5] and are available in versions 7.48 and later. The implementation is modeled on that of $W + jet$, the mass spectrum being adjusted to reflect the tower of graviton states rather than the virtual W.

The process is identified by the name EXTRADIM, and the keyword EXTRAD which expects parameters δ, M_D and a logical flag UVCUT. The last of these implements a cut off in the cross-section for large values of the partonic center of mass energy. If the result depends strongly on this variable, then the resulting rates are sensitive to physics above the scale M_D and the calculations are unreliable. This is discussed in more detail in section 3.2. The transverse momentum and mass range of the produced graviton is specified using the QTW and QMW parameters. Here is an example:

[‡]The cancellation of the $\bar{M}_P^2$ factor has already been taken into account in eq. 1

```
TEST EXTRADIM G+jet
14000,5000,10,100/
EXTRADIM
QMW
5,1000/
QTW
500,1000/
EXTRAD
2,1000,FALSE/
END
STOP
```

```
TEST EXTRADIM G+photon
14000,5000,10,100/
EXTRADIM
QMW
5,1000/
QTW
500,1000/
JETTYPE3
'GM'/
EXTRAD
2,1000,FALSE/
END
STOP
```

Table 1: Examples of data cards to generate graviton signals: $G + jet$ (left) and $G + \gamma$ (right).

2.3 Parameter ranges

The model has two parameters, the number of extra-dimensions δ and the fundamental scale M_D, for which some constraints already exist. The reader is referred to Ref [4] and references therein for further details. The case $\delta = 1$ is already excluded since it would imply deviations of the Newton law of gravitational attraction at distance scales that have already been explored. The case $\delta = 2$ is not very likely because of cosmological arguments. In particular graviton emission from Supernova 1987a [6] implies that $M_D > 50$ TeV. Large values of δ (> 6) can not be probed at LHC because the cross-section for graviton emission is too small. The lower value of M_D that can be considered is determined by two factors. It should be larger than the current limit from similar processes at the Tevatron. Furthermore it should also be large enough so that there are no significant contributions from the parton-parton center of mass energies where the effective theory is not appropriate. This is discussed in section 3.2.

3 Jet plus missing energy signature

The signal $pp \rightarrow jet + \not{E}_T$ is the most promising one for the direct graviton production at LHC. The dominant sub-process is $qg \rightarrow qG$. The following cases have been studied:

- δ = 2,3,4
- $M_D = M_D^{min}, \ldots, 5, 6, \ldots, 10$ TeV

Event generation has been performed with ISAJET as explained above. The default set of structure function has been used (CTEQ3L). Each sample consists of 60000 events generated in p_T^{jet} bins and re-weighted. The background samples have been generated in the same way and consist each of 300000 events.

3.1 Simulation with ATLFAST

The ATLAS detector was simulated using ATLFAST v2.22 [7] with the default values[§] for low and high-luminosity operation. However the transverse energy threshold to accept a calorimeter cluster

[§]It should be noted that to obtain the correct missing energy spectrum, the code for the SUSY LSP particle in ATLFAST (LPAR6 parameter) has to be set to 39, which is the graviton code.

as a jet has been raised from 15 GeV to 30 GeV. The jet algorithm used is the cone algorithm with a size $\Delta R = 0.4$. A larger cone size ($\Delta R = 0.7$) was also used but did not lead to any improvement. In order to better estimate the direction of the jets, which could be useful to fully take advantage of the typically back-to-back topology of the signal events, the use of the k_T jet algorithm has been investigated but no significant improvement was found.

3.2 Effective theory and validity range for M_D

It is important to note that the theory [4] is an effective low-energy theory, valid below the fundamental scale M_D. The behavior above M_D is not known, neither is the exact scale at which the theory breaks down. To assess the applicability of the effective theory, we checked whether the standard cross-section for the process is comparable to the truncated one where contributions from the high energy region are suppressed. By comparing the results obtained by using Equation 1 with those from the truncated form, the region of parameters where the results are reliable can be determined; if the results are the same then there is no sensitivity to the high energy region where new physics must enter. In Ref. [4] the partonic cross-section is truncated by setting it to zero when the partonic center of mass energy ($\sqrt{\hat{s}}$) exceeds M_D. In the ISAJET implementation a less drastic approach is taken; if the variable UVCUT is set then the rate given by Equation 1 is reduced by a factor of $M_D^4/\hat{s}^2$ when $\hat{s} > M_D^2$. The following set of figures illustrate the issues and allow us to determine the range of parameters in which the theory is applicable. Fig. 1 shows the rates for $\delta = 2$ using the cut off of Ref. [4] and those using the prescription in ISAJET. The same quantities for $\delta = 4$ are also shown on this figure.

For fixed values of M_D and δ there is a maximum value of jet E_T for which the results are reliable. Alternatively, for a fixed number of expected events or fixed value of E_T^{cut}, there is a value of M_D below which the results are not reliable. If there are expected to be significant events in this region where the truncated and untruncated models disagree, then the experiment is sensitive to new physics appearing at scales M_D and one can expect that other signals will appear. Fig. 2 shows the event rate as a function of M_D and can be used to determine this region. The figure shows that the minimum value of M_D increases with δ. For larger values of δ, M_D must be small in order that the signal be visible above the standard model backgrounds. These small values of M_D are below the minimum value, hence no model independent prediction is possible and $\delta \geq 5$ is not considered here.

3.3 Backgrounds

At the large values of missing E_T that are being considered, the dominant backgrounds arise from processes that can give rise to neutrinos in the final state, *viz.* $jet + Z(\rightarrow \nu\nu)$, $jet + W(\rightarrow \tau\nu)$, $jet + W(\rightarrow \mu\nu)$ and $jet + W(\rightarrow e\nu)$. We veto events where there is an isolated lepton within the acceptance of the ATLAS muon or tracking systems as this reduces the background from the last two sources. An isolated lepton is defined to be one that has less than 10 GeV of additional energy in a cone of radous $\Delta R = 0.2$ around the lepton's direction. Additional instrumental background can arise from events where jet energies are badly measured or energy is lost in cracks or beyond the end of the calorimeter. Studies [8] have shown that this effect is very small for large values of missing E_T that are relevant here and we neglect it.

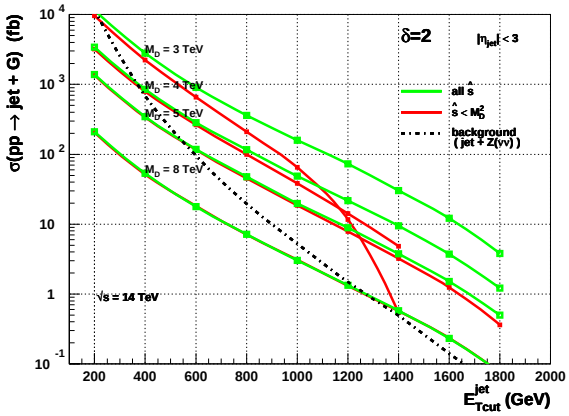

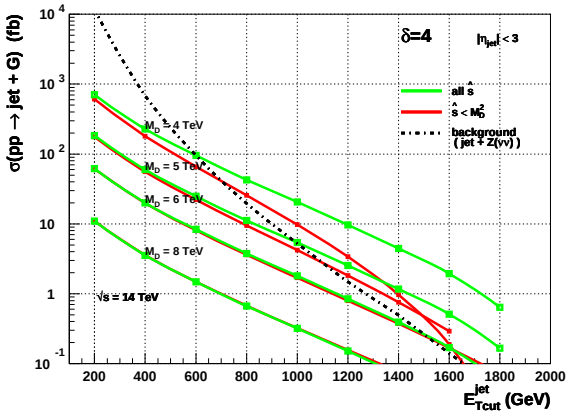

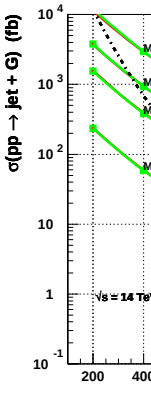

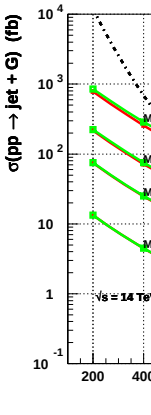

Figure 1: The integrated cross-section $\int_{E_T>E_T^{cut}} \frac{d\sigma}{dE_T} dE_T$, for the extra dimensions processes leading to the production of a jet of transverse energy E_T in association with missing transverse energy at LHC energy. 2 (top plots) and 4 extra dimensions are (bottom plots) are used and the curves are labelled by the values of M_D. The dashed line shows the main standard model background. The solid black lines show the effect of truncating the process according to the prescription of Ref. [4] (left plots) or following the approach implemented in ISAJET (right plots).

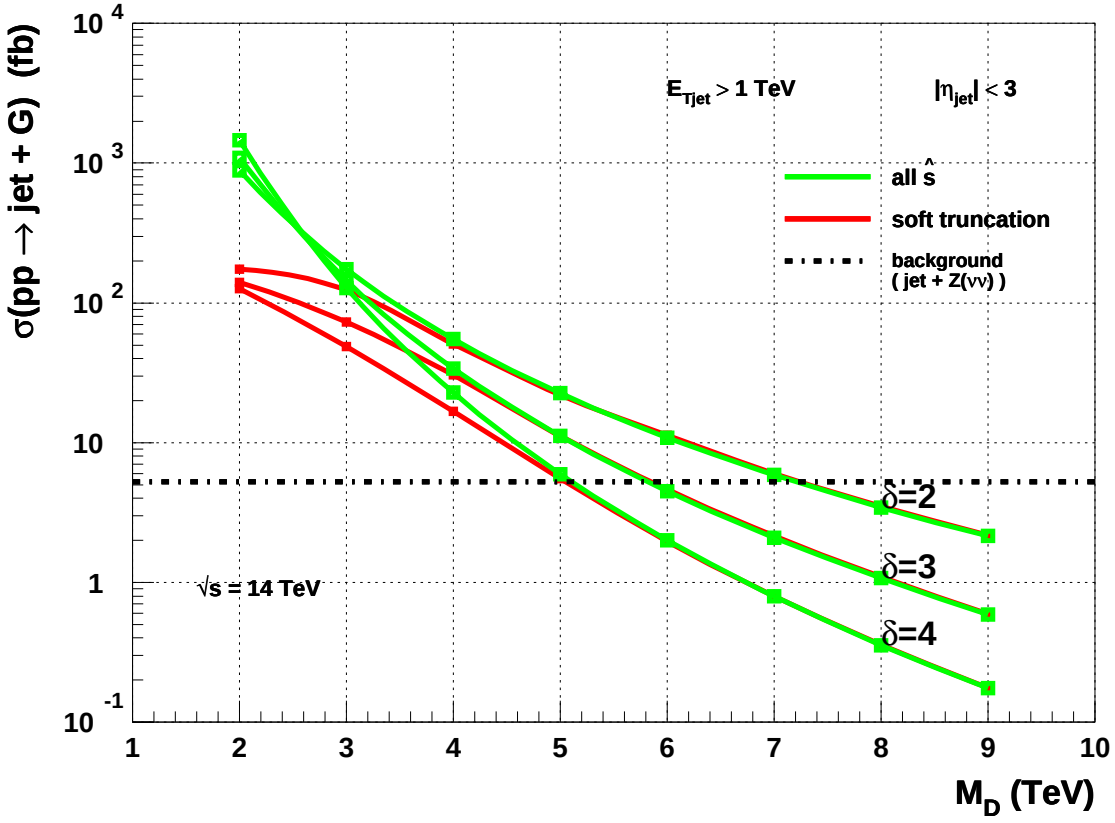

Figure 2: Cross section for jets with $E_T > 1$ TeV as function of M_D and δ at 14 TeV. ISAJET is used with UVCUT set to true (dark lines) and false (light lines). The horizontal line corresponds to the standard model background which is approximately 500 events with full luminosity (100 fb^{-1}).

3.4 Event Selection and Analysis

After the trigger selection, the lepton veto is applied. Additional selection relies on the topology of the events: missing transverse momentum, missing transverse momentum and leading jet back-to-back. A cut to remove the hadronic decays of the τ is also described.

If the values of M_D and δ are such that we are at the limit of sensitivity, *i.e* the signal and the background are comparable after missing E_T cuts, one can try to exploit these topological differences. We will demonstrate that while differences are expected they are too small to be of significance.

3.4.1 Trigger

The trigger is based on a combination of missing energy and jet. At low luminosity, a jet within the trigger acceptance ($|\eta| < 3.2$) and with $p_T \geq 50$ GeV is required, in addition to at least 50 GeV of missing transverse energy. At high luminosity, both thresholds are raised to 100 GeV. If needed, a higher threshold for $\not\!\!E_T$ could be used without affecting the study since the extraction of the signal relies on event rates at very large values of $\not\!\!E_T$ (of the order of one TeV). A global efficiency for this selection has been applied, using a conservative figure of 90%. It should be noted that this selection has been performed on the quantities reconstructed by ATLFAST which can slightly differ from the more crudely reconstructed ones at the trigger level.

3.4.2 Lepton veto

Events with an isolated lepton are vetoed, mainly to reduce the contribution of the jet+W background where the W decays leptonically. The acceptance for such isolated leptons is defined in ATLFAST as follows:

Electron: $p_T > 5$ GeV/c, $|\eta| < 2.5$

Muon: $p_T > 6$ GeV/c, $|\eta| < 2.5$

The distributions of the number of isolated lepton in the signal and in the backgrounds are shown on Fig. 3. A conservative value of $\epsilon_{veto} = 98\%$ for the lepton veto efficiency has been included by re-weighting the events by $(1 - \epsilon_{veto})^{n_{leptons}}$. No provision has been made for difference in the identification efficiency for electrons and muons. The veto retains 99.8% of the signal events while rejecting 23.3%, 74.3% and 61.1% of the $jW(\tau)$, $jW(e)$ and $jW(\mu)$ background events respectively.

3.4.3 Topology

The topology of the graviton+jet signal is quite simple (Fig. 4): a mono-jet which is back-to-back in azimuth to balancing missing transverse momentum. Additional jets arise from initial and final state QCD radiation. In the background events, a W or Z is emitted whereas in the signal events it is one of the tower of gravitons. The mass of this graviton can be large as the density of states increases exponentially with the mass and a typical emission can therefore have a mass larger than that of the W. The amount of QCD radiation is controlled by the total energy in the partonic system. For production at fixed E_T, we expect that there is more energy in the signal process due to the larger mass and therefore more QCD radiation which should manifest itself in increased jet multiplicity. In addition the backgrounds arise from initial states consisting mainly of $quark-gluon$ collisions, whereas the signal receives contributions from $gluon-gluon$ initial states. The greater color charge of the latter again tends to produce more radiation in the signal events.

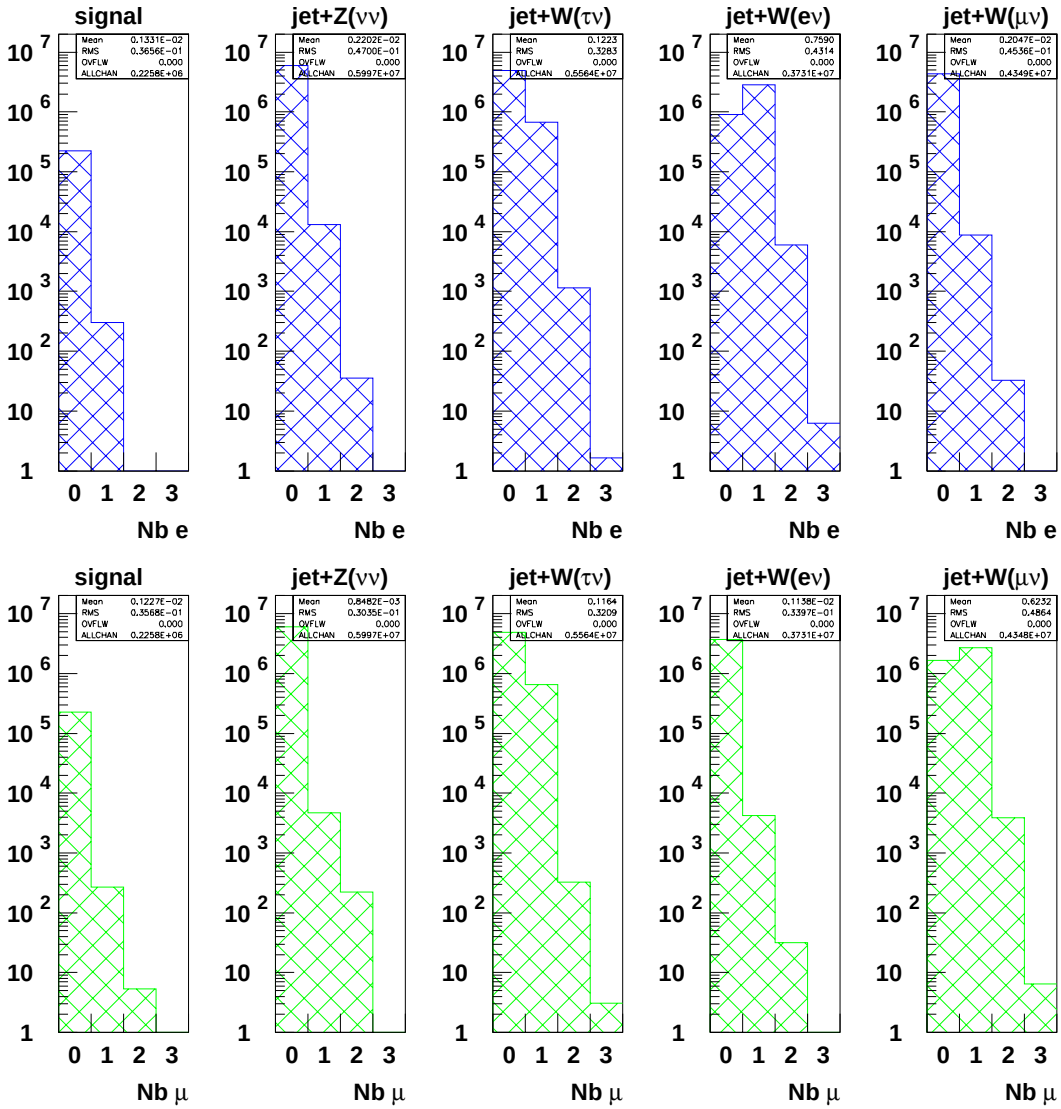

Figure 3: Distribution of the number of isolated electrons and muons after trigger cuts for the signal (in this case $\delta = 2,\ M_D = 5$ TeV) and for the backgrounds, for 100 fb^{-1}.

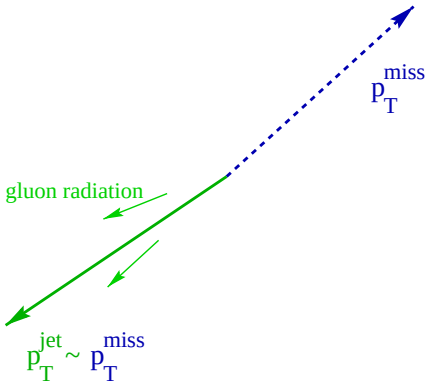

Figure 4: Sketch of a typical jet+G event.

The distribution of the number of jets in the events is shown in Fig. 5 for different kinds of signal and in Fig. 6 for the background events. As expected the average number of jets in the signal events is larger although the difference is small. The average number of jets increases significantly for large missing E_T: an average of 4 jets if $\not\!\!E_T$ is larger than one TeV. However, the difference between signal and background is very small for such high values of $\not\!\!E_T$.

The transverse energy distribution of the jet with highest E_T is shown in Fig. 7. This distribution is strongly correlated with the missing transverse energy in the event. Only the latter will be used for the selection. The pseudo-rapidity distribution of the leading jet (Fig. 7, right) does not allow discrimination between the signal and the backgrounds: in both cases, the jet is rather central. At lowest order in QCD the missing transverse momentum is back to back in azimuth with the leading jet. QCD radiation smears this as can be seen in Fig. 4 which shows the difference between the azimuthal angle of the leading jet and the angle of the missing transverse momentum. The differences between signal and background are too small to be useful.

In the signal events and in most of the backgrounds, the second jet is predominantly localized in the opposite hemisphere of the missing transverse energy: the leading jet as well as the other ones induced by gluon radiations and $\vec{\not\!\!p}_T$ are back-to-back in azimuth. However this is not the case in the $jet + W(\rightarrow \tau\nu)$ events, where hadronic decays of the taus can induce some hadronic activity on the same side of the missing momentum. This feature remains after a large cut on the missing transverse energy, as shown on Fig. 9 and can be used to reduce the background from $W \rightarrow \tau\nu$. A requirement that $\delta\phi(\vec{\not\!\!p}_T, jet_2) \geq 0.5$ rejects 6% of the signal events, 27% of the $jW(\tau\nu)$ events and 11% of all the background.

Finally, Fig. 10 shows the missing transverse energy distribution of the signal and backgrounds. The dominant background arises from the $jZ(\nu\nu)$ final state; $jW(\tau\nu)$ being the next most significant. Fig. 11 shows the missing transverse momentum distributions for several choices of δ and M_D; the signal can be seen to emerge from the background at large E_T^{miss}. These show the expected scaling of the cross-section as a function of $M_D^{-\delta-2}$.

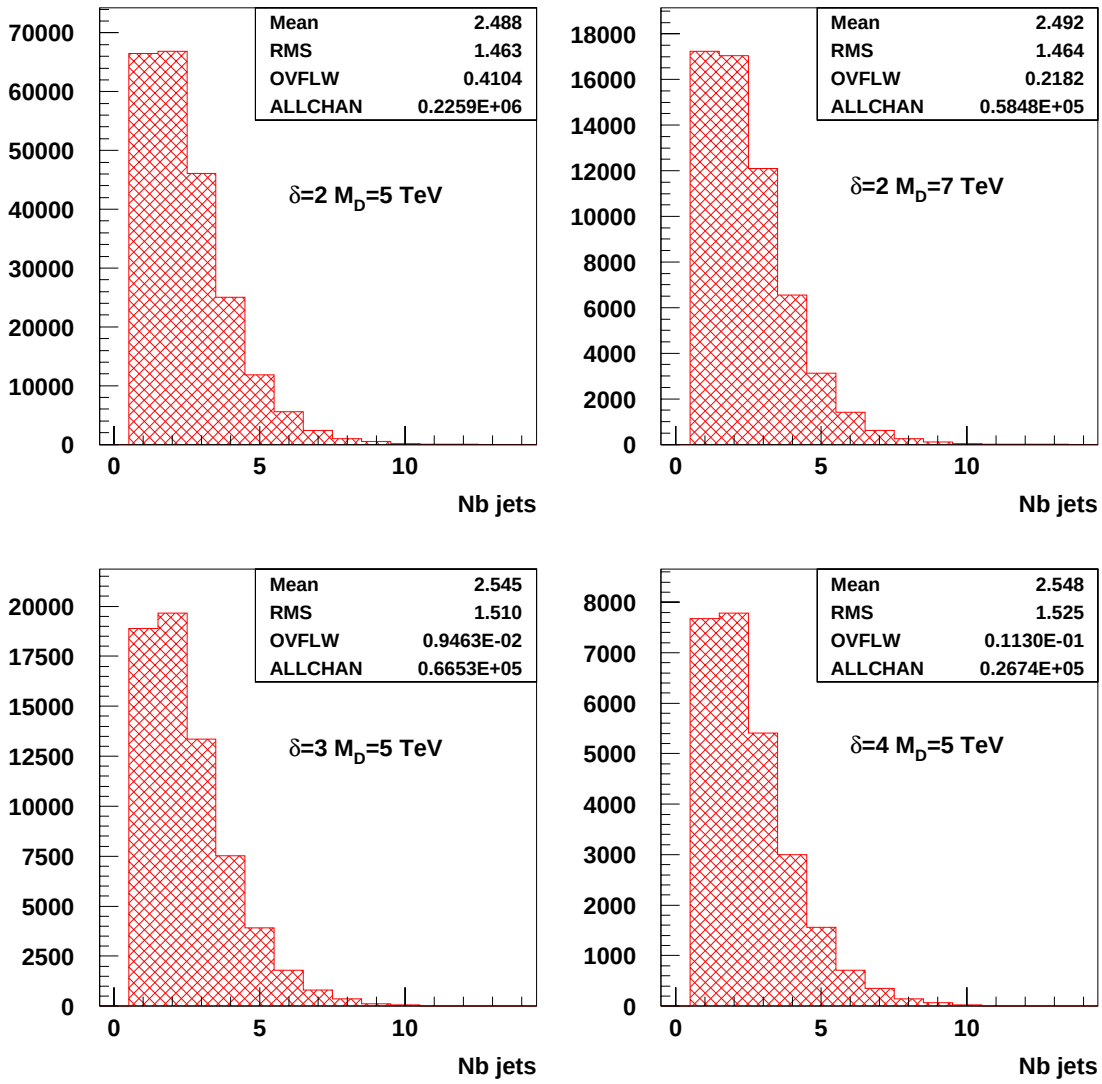

Figure 5: Distribution of the number of jets for different kinds of signal events after the trigger and for one year at high luminosity.

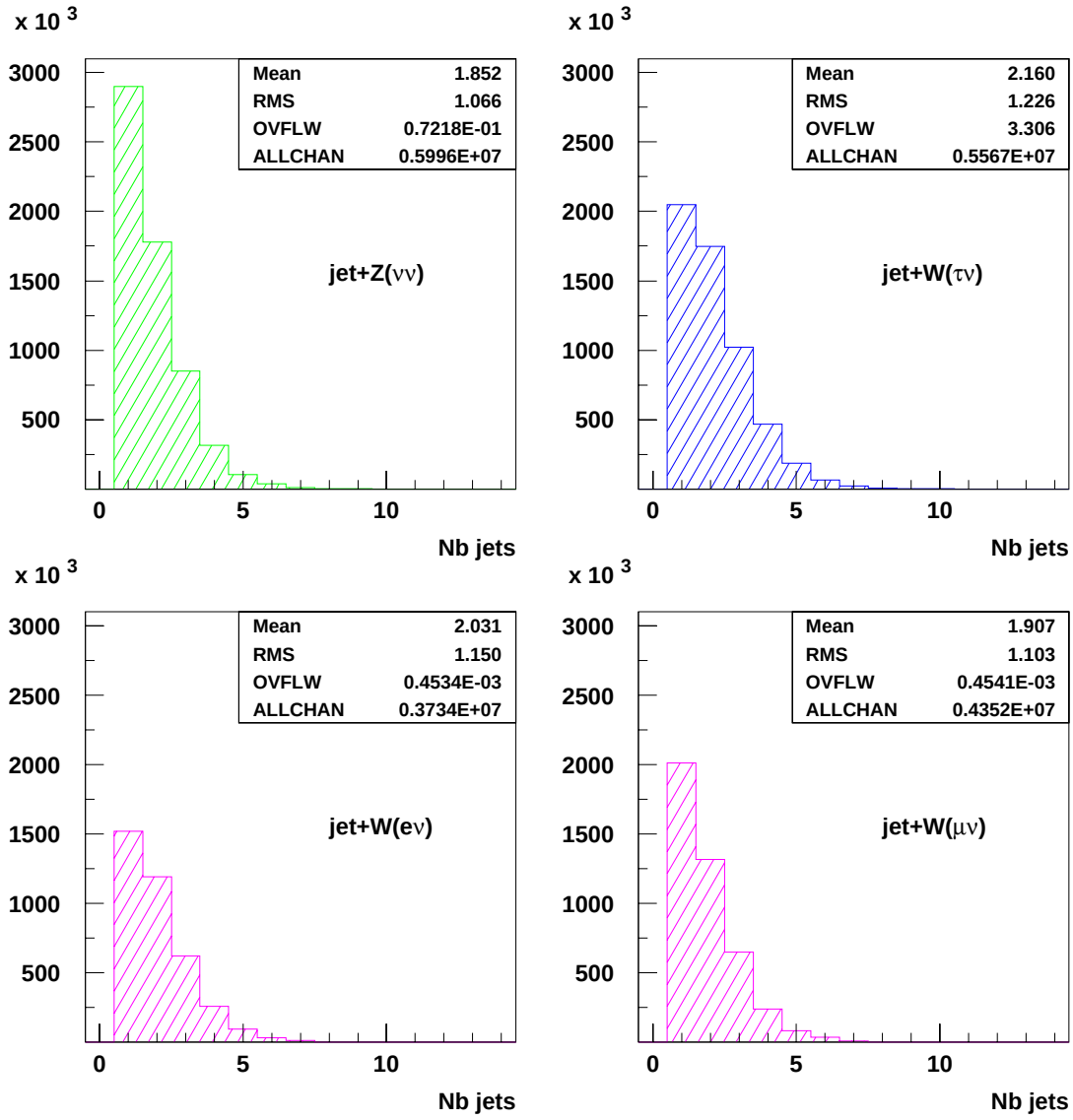

Figure 6: Distribution of the number of jets for the backgrounds after the trigger and for 100 fb^{-1}.

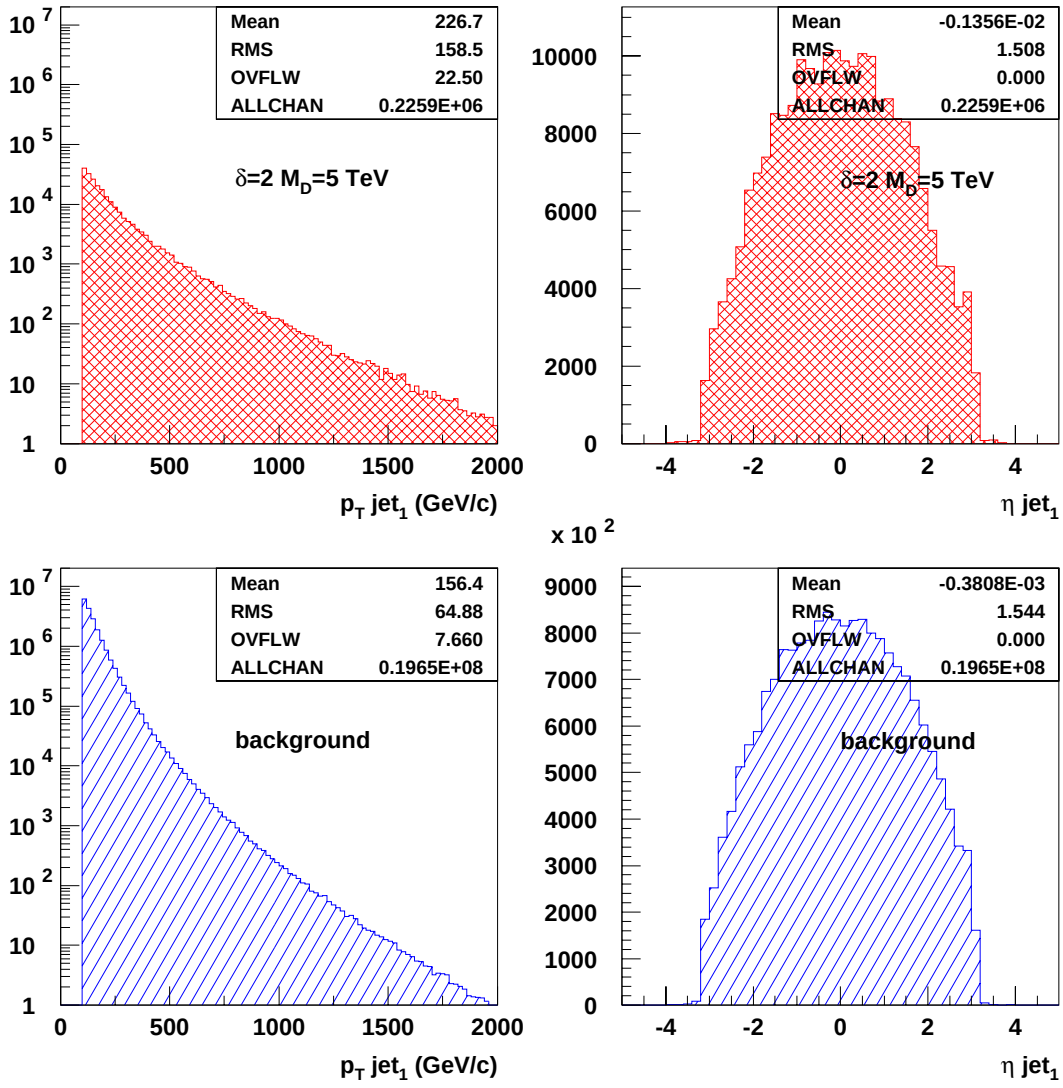

Figure 7: Distributions of the transverse momentum (left) and of the pseudo-rapidity (right) of the leading jet in signal events (top) and for all the backgrounds summed up (bottom), after the trigger and for 100 fb^{-1} of integrated luminosity.

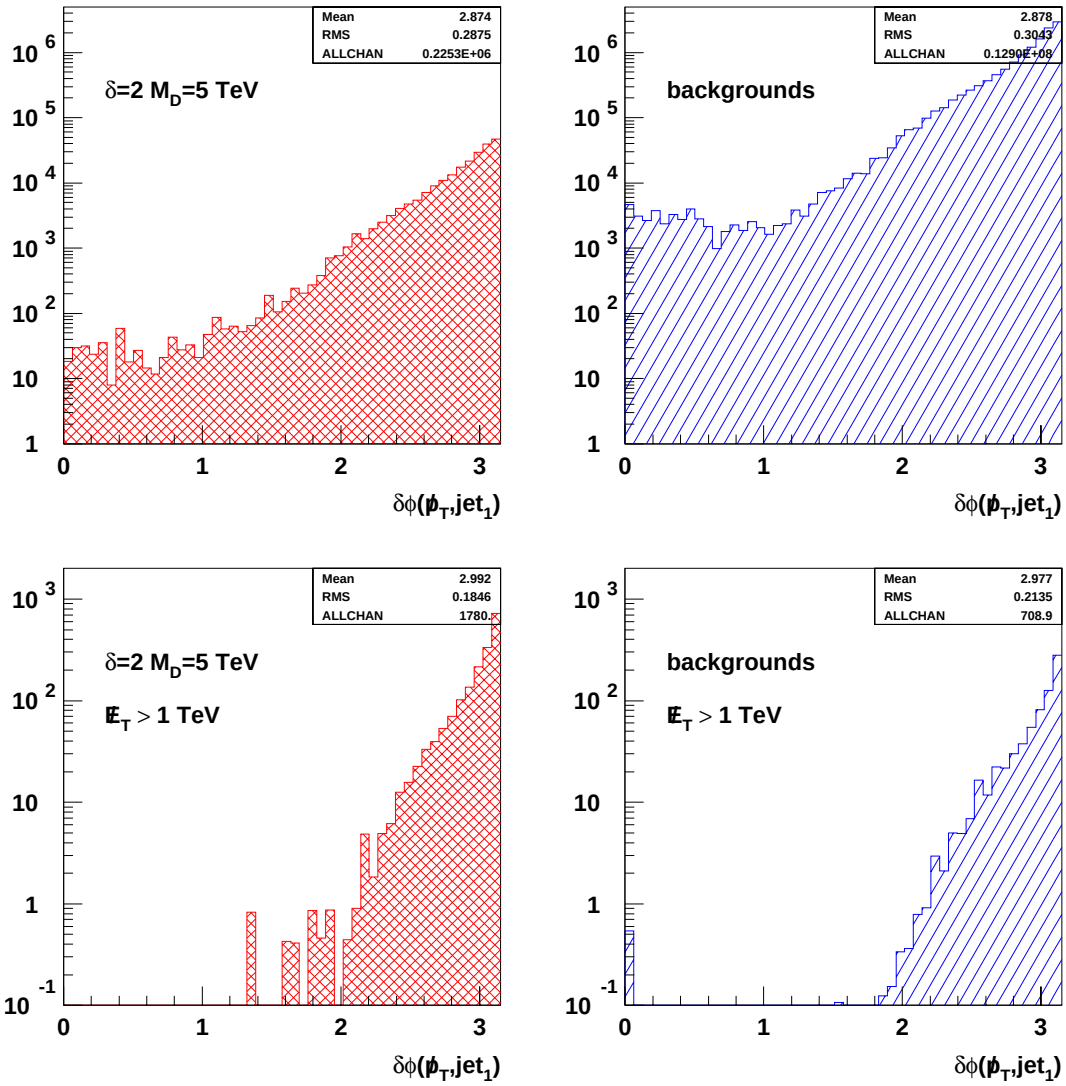

Figure 8: Distributions of the azimuthal angle difference $\delta\phi(\vec{\not{p}}_T, jet_1)$ between the missing transverse momentum and the leading jet in signal events (left) and in background events (right) for 100 fb^{-1}. The top distributions are after the trigger and the lepton veto while the bottom ones include in addition a cut on the missing transverse energy: $\not{E}_T > 1$ TeV.

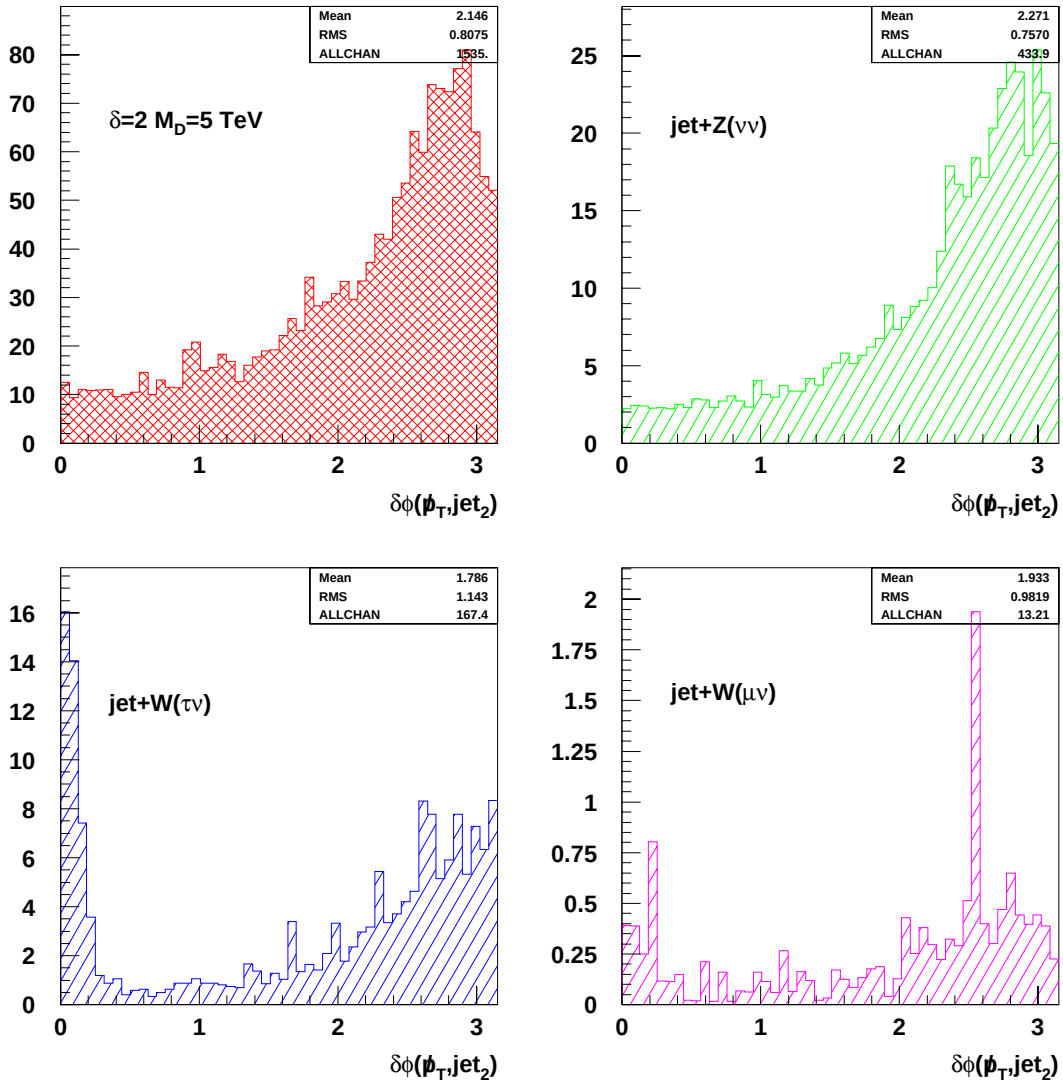

Figure 9: Distributions of the azimuthal angle difference $\delta\phi(\vec{\not{p}}_T, jet_2)$ between the missing transverse momentum and the second jet in signal and in background events, after the cut $\not{E}_T > 1$ TeV and for 100 fb^{-1}.

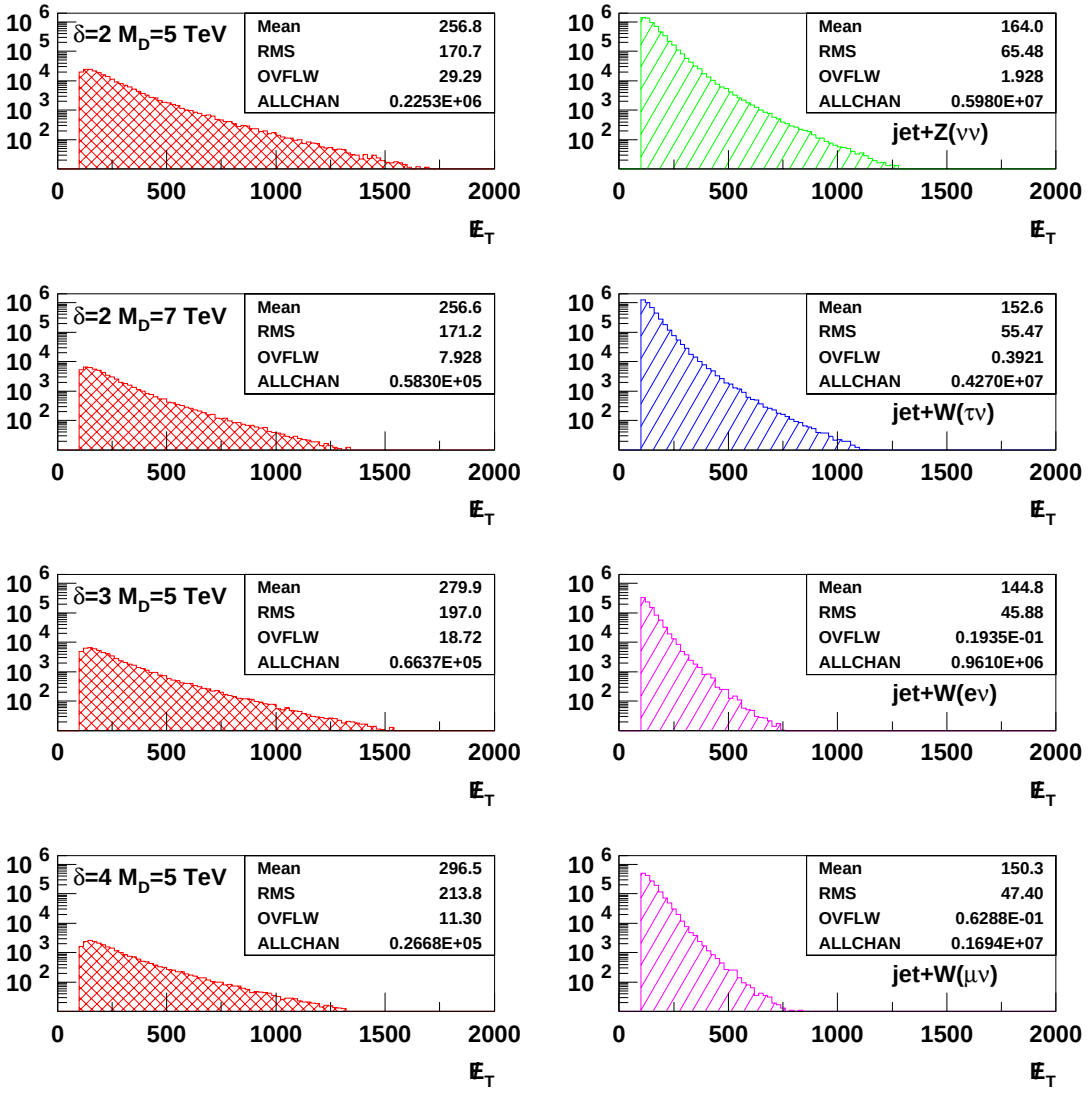

Figure 10: Distributions of the missing transverse energy in signal events (left) and in background events (right) after the trigger and the lepton veto and for 100 fb^{-1}.

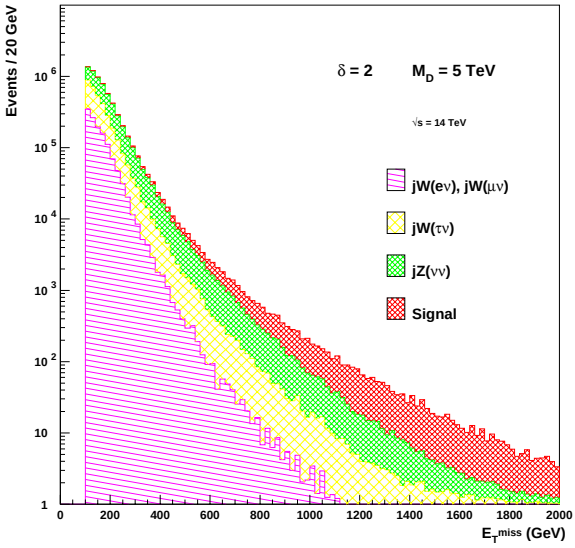

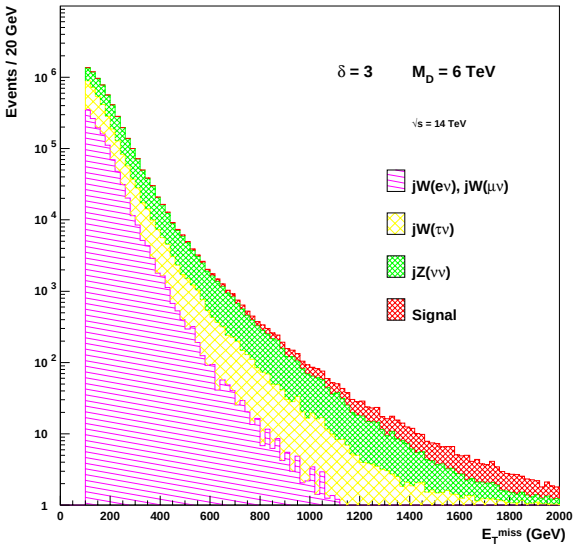

Figure 11: Distributions of the missing transverse energy in signal and in background events after the selection and for 100 fb^{-1} of integrated luminosity. Various cases (δ, M_D) for the signal are shown.

3.5 Sensitivity

In this section we estimate the sensitivity of ATLAS to δ and M_D. The background is dominated by the $jZ(\nu\nu)$ events which can be calibrated using events with electronic and muonic decays of the Z. Since $Br(Z \to \nu\nu) \sim 3[Br(Z \to \mu\mu) + Br(Z \to ee)]$ and the acceptance for muons and electrons from Z is not complete the size of this sample is smaller than the background and hence, if it is used to normalize the background, the error is larger than the naive estimate of the square root of the number of expected background events.

The ratio between the background and the calibration samples has been studied by simulating and applying a basic selection on $jZ(\to ee)$ events. For triggering we required one jet of at least 50 (100) GeV at low (high) luminosity within the trigger acceptance ($|\eta| < 3.2$) and two isolated electrons of at least 15 (20) GeV within $|\eta| < 2.5$. The invariant mass of the two electrons is required to lie in $m_Z \pm 10$ GeV.

Assuming that the $jZ(\to \mu\mu)$ sample can also be used, the calibration sample can be doubled. It can be seen from Fig. 12 that the calibration sample is approximately a factor of 7 smaller than the background sample. We therefore used $S/\sqrt{7B}$ as a statistical estimator of the signal significance. This is a worst case scenario; in practice the many measurements at LHC will give one confidence in predicting the missing transverse energy rate in the signal region.

Table 2 shows the number of signal and background events remaining after the selections. The statistical significance of the signal is shown in Tables 3, 4 and 5 for various choices of the cut on missing E_T.

$\not{E}_T >$	Type	Low luminosity, $30 fb^{-1}$	High luminosity, $100 fb^{-1}$
1 TeV	$jZ(\nu\nu)$	120.6	414.0
	$jW(\tau\nu)$	34.5	122.7
	$jW(e\nu)$	2.7	8.8
	$jW(\mu\nu)$	3.3	11.0
	Total	161.1	556.5
1.2 TeV	$jZ(\nu\nu)$	36.1	124.7
	$jW(\tau\nu)$	9.2	30.1
	$jW(e\nu)$	0.6	2.0
	$jW(\mu\nu)$	0.9	2.9
	Total	46.9	159.7
1.4 TeV	$jZ(\nu\nu)$	11.1	37.4
	$jW(\tau\nu)$	2.8	9.6
	$jW(e\nu)$	0.1	0.6
	$jW(\mu\nu)$	0.2	0.8
	Total	14.3	48.4

Table 2: Number of remaining background events after the selection. Three different cuts on $\not{E}_T$ are shown.

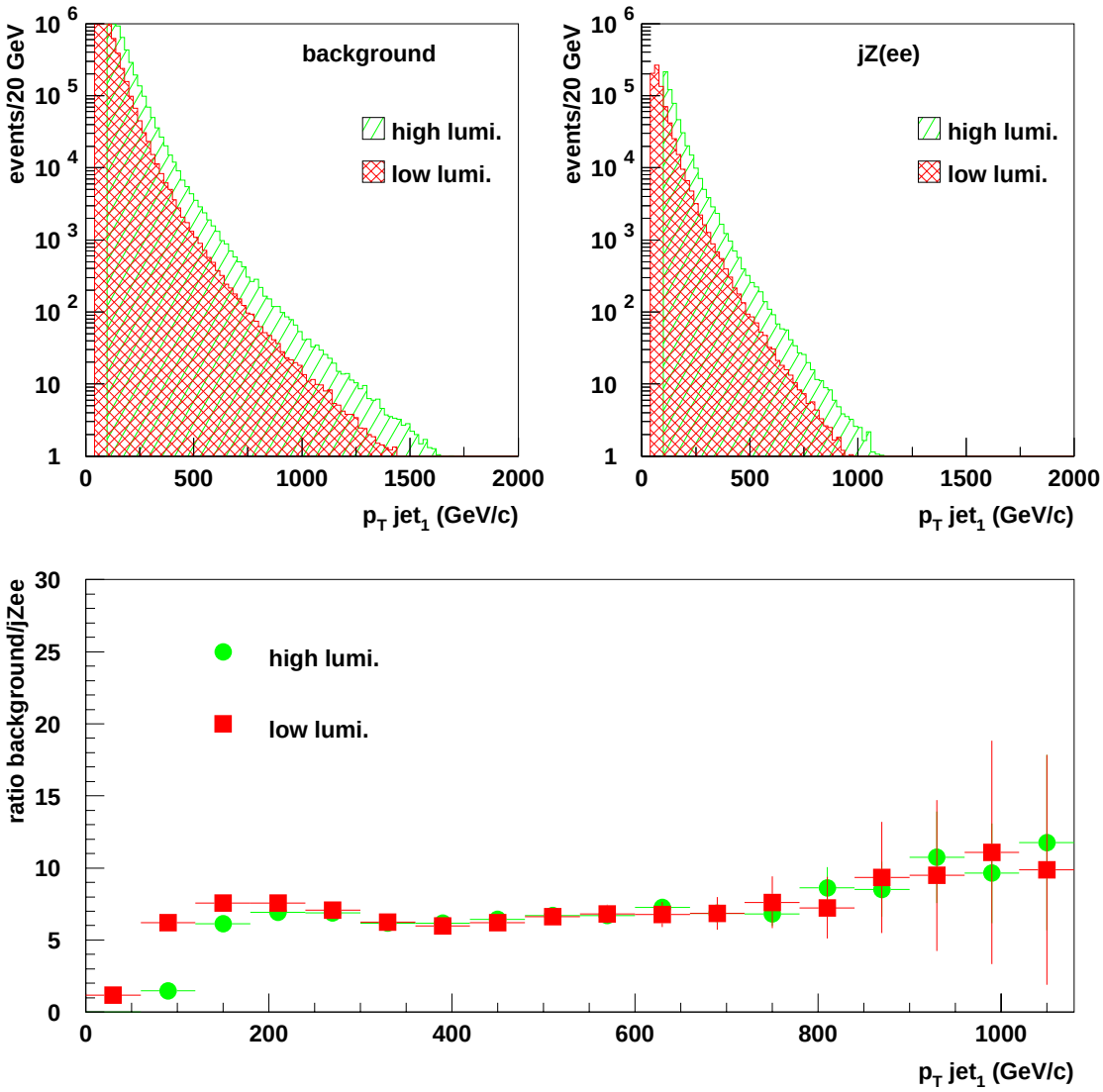

Figure 12: Distribution of the transverse momentum of the leading jet in background events (top left) and in the $jZ(\rightarrow ee)$ calibration sample (top right). The bottom plot shows their ratio (an extra factor of 0.5 has been included in the ratio to take into account the $jZ(\rightarrow \mu\mu)$ calibration sample).

δ	M_D	Low luminosity, $30fb^{-1}$			High luminosity, $100fb^{-1}$		
		S	$S/\sqrt{B}$	$S/\sqrt{7B}$	S	$S/\sqrt{B}$	$S/\sqrt{7B}$
2	4	1036.4	81.6	30.8	3542.2	150.2	56.8
	5	417.0	32.9	12.4	1426.9	60.4	22.8
	6	205.9	16.3	6.2	700.6	29.6	11.2
	7	111.3	8.8	3.3	379.4	16.1	6.1
	8	65.3	5.2	2.0	222.5	9.4	3.5
3	4	641.8	50.6	19.1	2168.4	92.0	34.8
	5	211.5	16.6	6.3	706.0	30.0	11.3
	6	85.1	6.8	2.6	287.5	12.1	4.6
	7	39.3	3.1	1.2	134.0	5.7	2.2
4	4	436.2	34.3	13.0	1473.4	62.5	23.6
	5	113.0	8.8	3.3	383.4	16.3	6.2
	6	37.8	2.9	1.1	128.5	5.4	2.0

Table 3: Number of remaining signal events after the selection ($\not{E}_T > 1$ TeV) and statistical significance.

δ	M_D	Low luminosity, $30fb^{-1}$			High luminosity, $100fb^{-1}$		
		S	$S/\sqrt{B}$	$S/\sqrt{7B}$	S	$S/\sqrt{B}$	$S/\sqrt{7B}$
2	4	463.8	67.7	25.6	1548.5	122.5	46.3
	5	186.2	27.2	10.3	622.8	49.4	18.7
	6	91.5	13.3	5.0	306.1	24.2	9.2
	7	47.3	6.9	2.6	163.9	13.0	4.9
	8	28.5	4.2	1.6	96.1	7.6	2.9
3	4	312.1	45.6	17.2	1050.0	83.1	31.4
	5	101.3	14.7	5.6	345.6	27.4	10.3
	6	40.9	5.9	2.2	139.2	11.1	4.2
	7	18.6	2.8	1.0	62.9	5.0	1.9
4	4	206.1	30.1	11.4	691.6	54.7	20.7
	5	54.0	8.0	3.0	184.1	14.5	5.5
	6	18.1	2.6	1.0	60.5	4.8	1.8

Table 4: Number of remaining signal events after the selection ($\not{E}_T > 1.2$ TeV) and statistical significance.

δ	M_D	Low luminosity, $30fb^{-1}$			High luminosity, $100fb^{-1}$		
		S	$S/\sqrt{B}$	$S/\sqrt{7B}$	S	$S/\sqrt{B}$	$S/\sqrt{7B}$
2	4	187.6	49.5	18.7	645.4	92.8	35.1
	5	77.6	20.4	7.7	272.8	39.1	14.8
	6	38.7	10.2	3.9	128.8	18.5	7.0
	7	19.7	5.2	2.0	66.5	9.5	3.6
	8	11.6	3.1	1.2	39.4	5.7	2.2
3	4	142.5	37.8	14.3	479.8	68.9	26.1
	5	46.2	12.3	4.6	159.8	23.0	8.7
	6	18.8	5.0	1.9	64.0	9.2	3.5
	7	8.5	2.3	0.9	29.4	4.2	1.6
4	4	97.1	25.6	9.7	324.4	46.6	17.6
	5	25.2	6.6	2.5	86.7	12.5	4.7
	6	8.6	2.3	0.9	28.4	4.2	1.6

Table 5: Number of remaining signal events after the selection ($\not{E}_T > 1.4$ TeV) and statistical significance.

Table 6 shows the maximum value of M_D and the corresponding size of the extra dimensions for various choices of δ to which ATLAS is sensitive. Values of M_D below the values shown will be discovered with at least 5σ significance. We have used the conservative statistical estimator in determining these values. The table also shows the value of M_D below which the event rates quoted here are not reliable and will be modified by the new physics appearing at scale M_D. Note that for $\delta = 4$ the two values of M_D are quite close; for larger values of δ the LHC sensitivity cannot be assessed using the signal that we have described and the limit of sensitivity is therefore model dependent.

δ	M_D^{min} (TeV)	M_D^{max} (TeV)	$R_{compact}$
2	~ 4	7.5	10 μm
3	~ 4.5	5.9	300 pm
4	~ 5	5.3	1 pm

Table 6: M_D ranges for which a 5-sigma discovery is possible after one year at high luminosity. R is the equivalent radius of compactification of M_D^{max}. The missing transverse energy was required to be larger than one TeV and $S/\sqrt{7B}$ was used as a statistical estimator.

4 Single photon signature

Another interesting signal at LHC is the production of the graviton in association with a photon. However the rates are much lower than in the graviton plus jet cases and the region of (δ, M_D) which can be probed is much more limited. We include a discussion here as this signature could be used as a confirmation after a discovery in the jet channel.

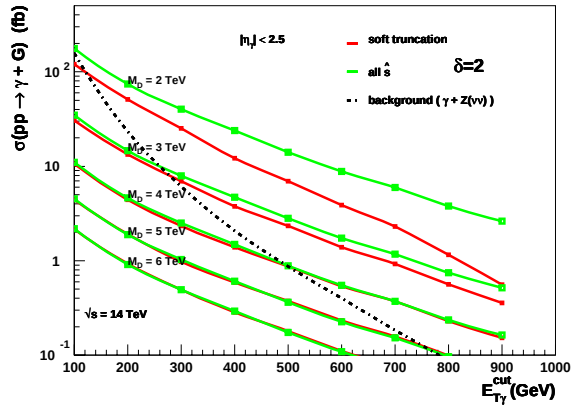

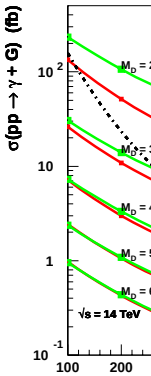

Figure 13: Integrated cross-section for the graviton plus photon signal as a function of the cut on the photon transverse energy for $\delta = 2$ (left) and $\delta = 3$ (right). The dashed line shows the main standard model background. The solid black lines show the effect of truncating the process in ISAJET.

4.1 Effective theory and validity range

To determine the validity range of the theory, we used the same method as described in section 2.3. Fig. 13 shows the cross-section $\sigma(pp \to \gamma G)$ as a function of the cut on the photon transverse energy ($\sim \not{E}_T$), for two extra-dimensions. The photon is required to be central ($|\eta| < 2.5$). The contribution of the main background ($\gamma + Z(\to \nu\nu)$) is also shown on the figure. The large differences between the standard cross-section and the truncated one ($\hat{s} < M_D^2$) for M_D below 4 TeV clearly show that the predictions are model dependent in this range. Unfortunately, the rates for $M_D \geq 4$ TeV are very low.

For three extra-dimensions, there is no region where the model independent predictions can be made and where the rate is high enough to observe signal events over the background (Fig. 13). The situation is of course even worse for larger values of δ.

4.2 Backgrounds

The main Standard model background is γZ where the Z decays into two neutrinos. PYTHIA 5.720 [9] has been used to generate 300 000 of these events. As in the jet case, the second most important background is the channel where a W boson is produced with the photon and where a large amount of missing energy can appear because of the W decay to $\tau\nu$. A sample of 300 000 events were generated with ISAJET.

Since the number of events with the other leptonic decays of the W ($e\nu$ and $\mu\nu$) which survived the lepton veto has been found to be negligible for the jet channel, those backgrounds have not been simulated for the photon channel.

4.3 Analysis

For triggering, at least one photon with $E_T > 60$ GeV at high luminosity and within $|\eta| < 2.5$ is required as well as at least 100 GeV of missing transverse energy. In addition, the lepton veto described in section 3.4.2 has been applied. As before the signal emerges from the background at large transverse missing energy: typically $\not\!\!E_T > 500$ GeV is required.

4.4 Sensitivity

To derive the sensitivity, a calibration sample of $\gamma Z(ee)$ events has been generated and selected as follows: in addition to a photon fulfilling the same trigger requirements as above, two electrons within $|\eta| < 2.5$ and with $p_T > 20$ GeV are required. The invariant mass of the two electrons has to lie within $m_Z \pm 10$ GeV. The calibration sample is 6 times smaller than the background sample. Therefore the statistical estimator used is $S/\sqrt{6B}$. The number of remaining background events after requiring that $\not\!\!E_T > 500$ GeV is summarized in table 7 for an integrated luminosity of 100 fb^{-1}. The number of signal events and the corresponding sensitivities are shown in Table 8.

$\not\!\!E_T >$	Type	High luminosity, $100 fb^{-1}$
500 GeV	$\gamma Z(\nu\nu)$	80.7
	$\gamma W(\tau\nu)$	2.2
	Total	82.9

Table 7: Number of remaining background events after the selection.

δ	M_D	High luminosity, $100 fb^{-1}$		
		S	$S/\sqrt{B}$	$S/\sqrt{6B}$
2	3	194.4	21.4	8.7
	4	61.8	6.8	2.8
3	4	49.2	5.4	2.2

Table 8: Number of remaining signal events after the selection and corresponding sensitivities. Various values of δ and M_D are shown.

As expected the sensitivity is very limited with this channel. Nevertheless it could provide a valuable check in case of a discovery in the jet channel, provided both the number of extra dimensions and the mass scale are not too large.

5 Summary and interpretation

Using the most conservative statistical estimator, the maximum value of the mass scale for which a 5-sigma discovery is possible has been derived, as well as the corresponding radius of the compactified space (assumed to be a torus). The results are summarized in Tables 9 and 10 for the jet and the gamma channels respectively.

δ	M_D^{min} (TeV)	M_D^{max} (TeV)	$R_{compact}$
2	~ 4	7.5	10 μm
3	~ 4.5	5.9	300 pm
4	~ 5	5.3	1 pm

Table 9: Mass scale ranges which can be probed at LHC for different number of extra dimensions using the jet plus missing transverse energy signature. The maximum value M_D^{max} corresponds to the highest mass scale for which $S > 5\sqrt{7B}$. $R_{compact}$ is the corresponding radius of compactification. M_D^{min} is an indicative value of the limit of reliability for the effective theory.

δ	M_D^{min} (TeV)	M_D^{max} (TeV)	$R_{compact}$
2	~ 3.5	3.7	30 μm

Table 10: Mass scale ranges which can be probed at LHC using the photon plus missing transverse energy signature. For $\delta > 2$ there is no value of M_D for which a model independent prediction is possible and the rate is high enough. The maximum value M_D^{max} corresponds to the highest mass scale for which $S > 5\sqrt{6B}$. $R_{compact}$ is the corresponding radius of compactification. M_D^{min} is an indicative value of the limit of reliability for the effective theory.

The quoted values for M_D^{min} are indicative of the limit of reliability for the effective theory: below M_D, some new physics may well occur. However it should be stressed again that a signal is not precluded in this region. Furthermore, it is possible to extend the interesting region to lower values of M_D by releasing the cut on the transverse missing energy (provided the background still remains under control).

If a signal is observed at LHC, one would like to measure the fundamental parameters M_D and δ. As can be seen from Fig. 14, using the shapes of these curves it is not possible to determine both δ and M_D; for example the curves for $\delta = 2$ and $M_D = 6$ TeV are very similar to those for$\delta = 3$ and $M_D = 5$ TeV.

In order to distinguish these, we must exploit the variation of the cross-section with the center of mass energy of the LHC. Fig. 15 shows the rates at a center of mass energy of 10 TeV. It can be seen that the rates for $\delta = 2$ and $M_D = 6$ TeV and $\delta = 3$ and $M_D = 5$ TeV differ by approximately a factor of two.

There is a kinematic limit (m^{max}) on the mass of the graviton that can be emitted. This limit depends on the the center of mass energy. of respectively 14 and 10 TeV. (cf. Eqn. 1). The ratio of cross-sections at different center of mass energies

$$\frac{\sigma(pp \to jet + G)_{\sqrt{s}=10\ TeV}}{\sigma(pp \to jet + G)_{\sqrt{s}=14\ TeV}}$$

is almost independent of M_D and varies with δ as can be seen from Fig. 16. The measured ratio should allow determination of the number of extra-dimensions, provided that the error is small enough. An experimental accuracy of the order of 5% on the ratio is needed to discriminate between $\delta = 2$ and $\delta = 3$. For $M_D = 6$ TeV and $\delta = 2$, the event rate at 10 TeV is approximately 1/3 of that at 14 TeV and, since the event rates are small, comparable integrated luminosity would be needed to measure the rate with sufficient statistical accuracy. Note that the relative luminosity of the LHC at the two energies would also need to be measured with comparable accuracy.

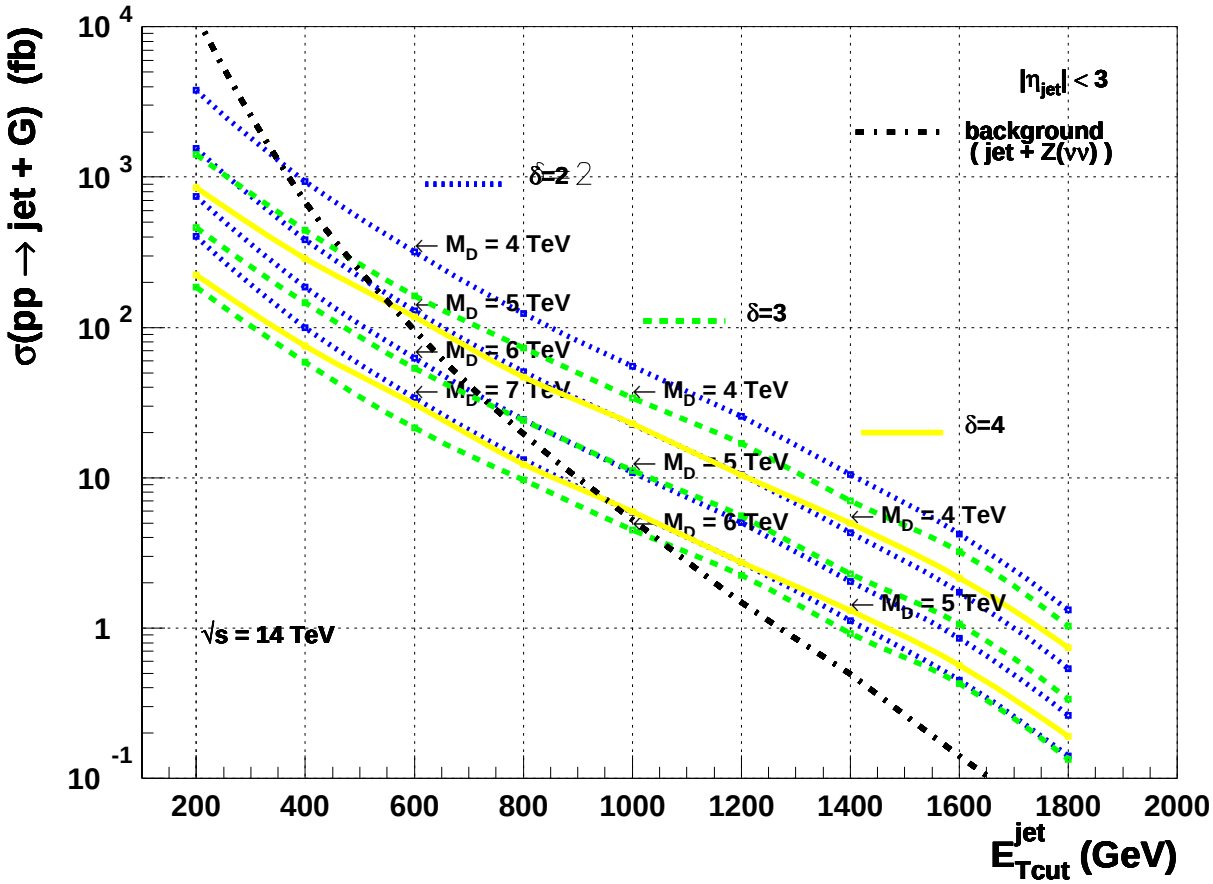

Figure 14: The integrated cross-section $\int E_T > E_T^{cut_{Tjet}}$, for the extra dimensions processes leading to the production of a jet of transverse energy E_T in association with missing transverse energy at LHC energy for various values of $\delta = 2$ and M_D. The dashed line shows the Standard model background.

To estimate the sensitivity for $\sqrt{s} = 10$ TeV, the same analysis as the one for the nominal LHC center-of-mass energy (page 8) has been performed. However only the 1 TeV cut on the transverse missing energy has been used. We assumed the same trigger and selection criteria and an integrated luminosity of $50 fb^{-1}$.

It can be seen from Fig. 15 that the available region in the (δ, M_D) parameter space is more limited than for a center-of-mass energy of 14 TeV. It is in particular not possible to look at the $\delta = 4$ case. Fig. 17 shows the distributions of the transverse missing energy as a function of the cut on the jet transverse energy.

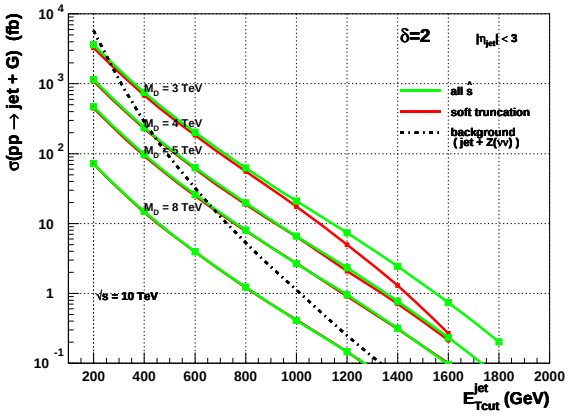

Figure 15: Integrated cross-section for the graviton plus jet signal as a function of the cut on the jet transverse energy for $\delta = 2$ (left) and $\delta = 3$ (right). The center of mass energy is 10 TeV.

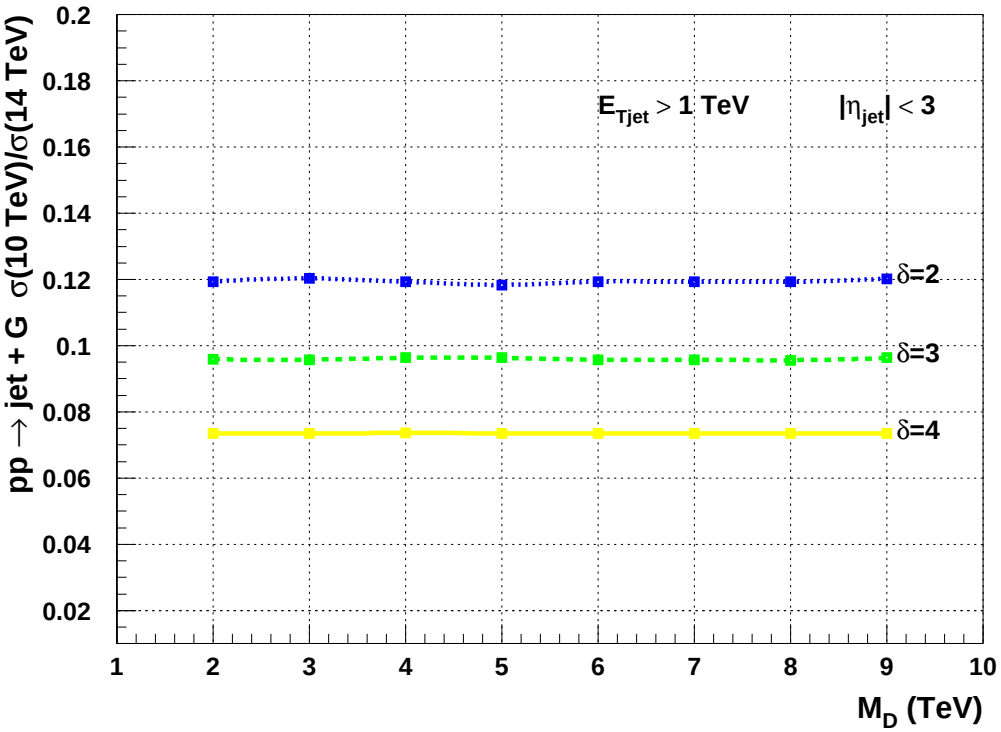

Figure 16: Distribution of the ratio of the cross-sections for the $pp \to jet + G$ signal at $\sqrt{s} = 10$ TeV and at $\sqrt{s} = 14$ TeV as a function of M_D and for different values of δ.

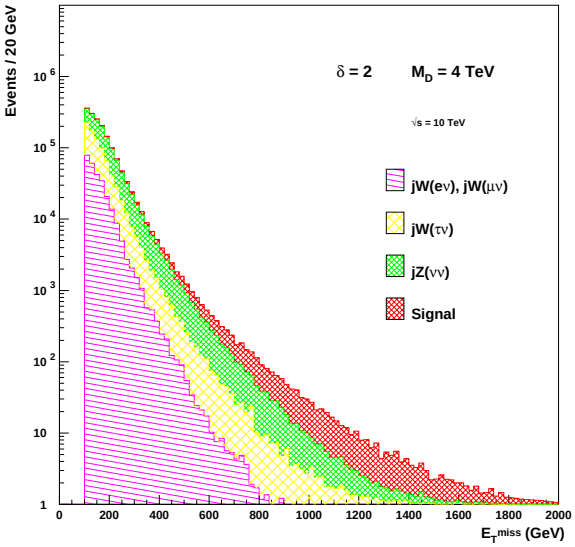

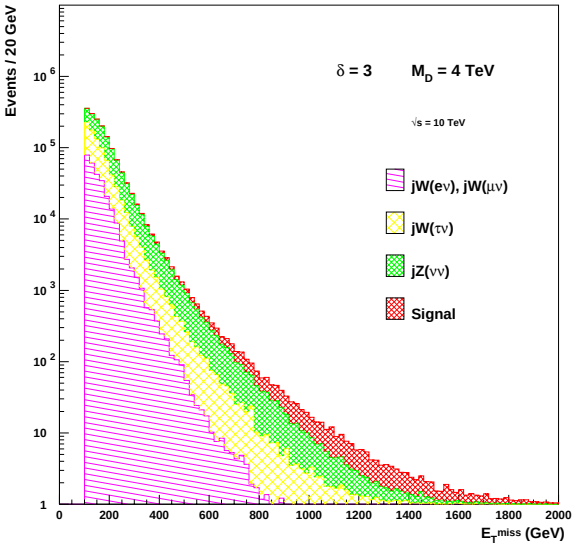

Figure 17: Distributions of the missing transverse energy in signal and in background events after the selection and for half a year at high luminosity and at $\sqrt{s} = 10$ TeV. Various cases (δ, M_D) for the signal are shown.

After the selection, the number of remaining background events and signal events are shown in table 11 and table 12 respectively. The sensitivity is derived using the same method as for the $\sqrt{s} = 14$ TeV case. However the normalization factor is a bit smaller (6) as the acceptance for Z decays to leptons is slightly larger. Note that the method is limited to $\delta \lesssim 3$ as the rates at 10 TeV are smaller.

$\not{E}_T >$	Type	High luminosity, $50 fb^{-1}$
1 TeV	$jZ(\nu\nu)$	41.4
	$jW(\tau\nu)$	11.9
	$jW(e\nu)$	1.5
	$jW(\mu\nu)$	1.6
	Total	56.4

Table 11: Number of remaining background events after the selection.

δ	M_D	High luminosity, $50 fb^{-1}$		
		S	$S/\sqrt{3B}$	$S/\sqrt{6B}$
2	4	175.2	23.4	9.5
	5	72.2	9.7	4.0
	6	34.3	4.5	1.8
3	4	86.5	11.6	4.7
	5	28.6	3.8	1.6

Table 12: Number of remaining signal events after the selection ($\not{E}_T > 1$ TeV) and statistical significance.

6 Other signatures

There are many other possible signals from theories of extra dimensions. These involve interactions due to new particles of masses of order M_D. The exchange of these particles between quarks and leptons can induce changes in the jet and Drell-Yan rates at LHC [10]. These signals are qualitatively the same as those for Compositeness (see for example, chapter 22 of the ATLAS Detector and Physics Performance Technical Design Report [11])

Another class of models have been proposed [12]. In this class there is no large hierarchy between R and $1/M_D$ and no tower of graviton states. In this case the class of signatures discussed in this note is absent.

Acknowledgments

This work was supported in part by the Director, Office of Science, Office of High Energy and Nuclear Physics, Division of High Energy Physics of the U.S. Department of Energy under Contracts DE-AC03-76SF00098. Accordingly, the U.S. Government retains a non-exclusive, royalty-free license to publish or reproduce the published form of this contribution, or allow others to do so, for U.S. Government purposes.

References

[1] N. Arkani-Hamed, S. Dimopoulos and G. Dvali, Phys. Lett. **B429**, 263 (1998)

[2] I. Antoniadis, Phys. Lett. **B246**, 377 (1990).

[3] M. B. Green, J. H. Schwarz and E. Witten, *Cambridge, Uk: Univ. Pr. (1987) 469 P. (Cambridge Monographs On Mathematical Physics)*. and refs theirin.

[4] G. F. Giudice, R. Rattazzi and J. D. Wells, Nucl. Phys. **B544**, 3 (1999)

[5] F. Paige and S. Protopopescu in *Supercollider Physics*, p. 41, ed. D. Soper (World Scientific, 1986);
H. Baer, F. Paige, S. Protopopescu and X. Tata, in *Proceedings of the Workshop on Physics at Current Accelerators and Supercolliders*, ed. J. Hewett, A. White and D. Zeppenfeld, (Argonne National Laboratory, 1993)

[6] S. Cullen and M. Perelstein, Phys. Rev. Lett. **83**, 268 (1999)

[7] E. Richter-Was, D. Froidevaux, and L. Poggioli, 'ATLFAST 2.0: a fast simulation package for ATLAS', ATLAS Internal Note ATL-PHYS-98-131 (1998).

[8] ATLAS "Detector and Physics Performance Technical Design Report", CERN/LHCC/99/14, Section 9.2.2 (1999).

[9] T. Sjostrand, Comput.Phys.Commun.82:74-90 (1994).

[10] J. L. Hewett, Phys. Rev. Lett. **82**, 4765 (1999)

[11] ATLAS Detector and Physics Performance Technical Design Report LHCC 99-14/15

[12] L. Randall and R. Sundrum, Phys. Rev. Lett. **83**, 3370 (1999)